AD_____

Award Number: DAMD17-02-1-0033

TITLE: Angiogenesis and Invasiveness in Prostate Cancer Detected with High Spectral and Spatial Resolution MRI

PRINCIPAL INVESTIGATOR: Gregory S. Karczmar, Ph.D.

CONTRACTING ORGANIZATION: University of Research Administration
Chicago, Illinois 60637

REPORT DATE: January 2005

TYPE OF REPORT: Annual

PREPARED FOR: U.S. Army Medical Research and Materiel Command
Fort Detrick, Maryland 21702-5012

REPORT DOCUMENTATION PAGE

Form Approved
OMB No. 074-0188

1. AGENCY USE ONLY (Leave blank)	2. REPORT DATE	3. REPORT TYPE AND DATES COVERED
	January 2005	Annual (24 Dec 2003 - 23 Dec 2004)

4. TITLE AND SUBTITLE
Angiogenesis and Invasiveness in Prostate Cancer Detected with High Spectral and Spatial Resolution MRI

5. FUNDING NUMBERS
DAMD17-02-1-0033

6. AUTHOR(S)
Gregory S. Karczmar, Ph.D.

7. PERFORMING ORGANIZATION NAME(S) AND ADDRESS(ES)
University of Research Administration
Chicago, Illinois 60637

E-Mail: gskarczm@uchicago.edu

8. PERFORMING ORGANIZATION REPORT NUMBER

9. SPONSORING / MONITORING AGENCY NAME(S) AND ADDRESS(ES)
U.S. Army Medical Research and Materiel Command
Fort Detrick, Maryland 21702-5012

10. SPONSORING / MONITORING AGENCY REPORT NUMBER

11. SUPPLEMENTARY NOTES

12a. DISTRIBUTION / AVAILABILITY STATEMENT
Approved for Public Release; Distribution Unlimited

12b. DISTRIBUTION CODE

13. ABSTRACT (Maximum 200 Words)

This grant is currently in a no- cost extension and we have made substantial progress on each of the specific aims of the proposal. In the last year, three papers were published in peer-reviewed journals describing work supported by this grant. In addition, there were four presentations at international meetings. Several grants have been funded based on preliminary results that were obtained with DAMD funding. Therefore, we will be able to continue this work, even though this is our last year of DAMD funding.

Substantial improvement in high spectral and spatial resolution data acquisition and processing were made. In addition, experimental data demonstrated that HiSS MRI shows novel anatomic features that are not detected by conventional MRI, both in human volunteers and in rodent models of prostate cancer. Statistical analysis demonstrates that lesion morphology is significantly different in HiSS images compared to conventional images, and in images of 'off-peak' Fourier Component images, compared to water peak height images.

During the final funding period, we plan to scan more volunteers and man with prostate cancer. In addition, we plan to extend our work on Fourier Component Imaging in order to demonstrate that this new approach to imaging provides unique contrast.

14. SUBJECT TERMS
Prostate MRI, spectral spatial imaging, prostate cancer, animal models

15. NUMBER OF PAGES
26

16. PRICE CODE

17. SECURITY CLASSIFICATION OF REPORT	18. SECURITY CLASSIFICATION OF THIS PAGE	19. SECURITY CLASSIFICATION OF ABSTRACT	20. LIMITATION OF ABSTRACT
Unclassified	Unclassified	Unclassified	Unlimited

Table of Contents

INTRODUCTION: Narrative that briefly (one paragraph) describes the subject, purpose, and scope of the research.

The goal of this research is to use high spectral and spatial resolution (HiSS) MR imaging to improve images of human and murine prostate. Our work on the application of HiSS to improve anatomic and functional imaging was first described in a paper in Academic Radiology [1]. Related work from this laboratory is presented in a number of other publications [2-9]. Work from other laboratories shows that closely related methods also provide advantages for anatomic [10] and functional [11-14] MRI.

This significant body of work provides support for the feasibility of ongoing experiments in this laboratory. Specifically, we expect to 1) improve separation of water and fat signals 2) increase image contrast 3) increase sensitivity to contrast agents and to local physiology – and as a result improve detection of suspicious lesions such as cancers and particularly delineation of tumor edges. We expect that this will increase the sensitivity and specificity of MR scans for prostate cancer. To achieve these goals our original 'statement of work' is summarized as follows:

A. Develop high spectral and spatial resolution (HiSS) magnetic resonance imaging (MRI): We will implement fast, high-resolution, high-spectral bandwidth imaging on a 4.7 Tesla (T) scanner. The 4.7 Tesla scanner will be upgraded with a next-generation control console during the next six months. K-space trajectories of HiSS pulse sequences will be corrected for eddy-current effects. Spectral data will be processed to obtain pure absorption spectra in which truncation artifacts are minimized in each voxel. Images will be synthesized in which intensity is proportional to water resonance peak height, line width, integral, resonance frequency, number of resolved components of the water signal, and other features of the water and fat signals. To test whether the methods are working properly we will image phantoms that are constructed to provide complicated structures with differing susceptibility. In addition, we will test the methods by imaging rat brains – the brain, unlike tumor tissue, has a precisely defined and well-characterized anatomy.

B. CAD (computer-aided diagnosis) techniques developed by Dr. Jiang and colleagues will be adapted for use with HiSS MRI datasets. The texture of images derived from HiSS datasets, i.e., the spatial variation in image intensity, will be measured quantitatively. Tumor edges will be analyzed to determine their degree of irregularity. Changes in HiSS data following contrast media injection will be measured. These methods will be developed iteratively and in parallel with MR studies of metastatic and non-metastatic rodent tumors (see below). Each new version of the CAD method will be evaluated based on its ability to discriminate between metastatic and non-metastatic tumors.

C. Evaluation of HiSS MRI and use of HiSS MRI to compare metastatic and non-metastatic rodent tumors implanted in murine hind limb and in murine prostate.

D. Studies of human prostate cancer: We will evaluate the accuracy of HiSS imaging of patients with prostate abnormalities.

BODY:

SOW A. During the last year – we have made the following technical improvements in our HiSS imaging:

1. Upgraded our EPSI sequence to run more efficiently on our new Bruker console. As a result, we were able to increase both spatial *and* spectral resolution. We are now acquiring images of animal models of prostate with spatial resolution of 125 micron in plane in 500 micron thick slices and spectral resolution of 5 Hz. In human volunteers we are acquiring multislice HiSS images with 1 mm in – plane resolution in 3 mm thick slices, and spectral resolution of 5 Hz.

2, *Increased data acquisition speed:* We implemented technical advances that will allow us to cut our run time for HiSS images by a factor of 4. Specifically we developed a new pulse sequence in which two or more lines of k-space are sampled in parallel, using phase encoding gradient 'blips' between the odd and even echoes. As a result, odd echoes sample one line of k-space and even echoes sample a neighboring line of k-space. We have also implemented parallel imaging in which signals from various coil elements are analyzed to avoid fold-back. This allows an additional decrease of a factor of 2. Both of these improvements have been tested in phantoms and work well. In the next few months they will be tested in a second group of volunteers.

3. Phased images: We developed a robust algorithm for producing phased spectra in each voxel. This increases the quality of both water peak height images and linewidth images. This algorithm has been tested in scans of human volunteers and animal models of prostate cancer (see below).

SOW B: We completed CAD work during the previous year and now have neural network methods that allow improved differentiation of metastatic and non-metastatic rodent prostate tumors. Dr. Jiang and his graduate student, Yahui Peng, also developed statistical methods for identifying optimal combinations of parameters derived from HiSS datasets for staging rodent cancers.

SOW C: We completed work to differentiate metastatic and non-metastic rodent prostate cancers using a combination of high temporal, spatial, and spectral resolution sampling. Two papers describing this work have been published and an additional manuscript is in preparation. Additional scans of rodent prostate tumors are currently underway to evaluate sensitivity to contrast media and further enhance our ability to stage tumors with HiSS MRI.

The two published papers are referenced below.

SOW D: Studies of human cancer: We performed 10 scans of volunteers and produced multislice HiSS images with in-plane spatial resolution of 1 mm in 2 mm thick slices. We are now working on producing images from phased water spectra, and using these images to calculate maximum intensity projection images. We have also developed a collaboration with Drs. Hania Al-Hallaq and Ashesh Jani in Radiation and Cellular Oncology to scan patients who have prostate cancer. We expect to begin scanning these patients in June.

KEY RESEARCH ACCOMPLISHMENTS: Bulleted list of **key** research accomplishments emanating from this research

- We demonstrated advantages of HiSS imaging of orthotopic prostate cancer in mouse and completed a paper describing this work – which is now in press in NMR in Biomedicine.

- We implemented important technical advances on our whole body scanner – parallel imaging and parallel sampling of multiple k-space lines that will speed up data acquisition. We also developed an improved algorithm for spectral phasing, and peak height, T2*, and Fourier component images produced with this algorithm are greatly improved.

- Performed 10 scans of normal volunteers – some of these scans included multi-slice HiSS imaging.

- Made further progress on Fourier component imaging. In particular we showed statistically significant differences in rodent prostate tumors between images derived from the off-peak Fourier components of the water resonance and water peak height images. These results are described in the attached manuscript in progress.

REPORTABLE OUTCOMES:

Peer reviewed papers:

1) M Medved, G Newstead, X Fan, W Du, Y Du, P MacEneaney, RM Culp, F Kelcz, O Olopade, M Zamora, G Karczmar. Fourier Components of Inhomogeneously Broadened Water Resonances in Breast: A New Source of MRI Contrast. Magn Reson Med **52:** 193-196 (2004).

2) Du W, Fan X, Foxley S, Zamora M, River JN, Culp RM, and Karczmar GS. Comparison of high resolution echo-planar spectroscopic imaging with conventional MR imaging of prostate tumors in mice. Manuscript in preparation for NMR in Biomedicine.

3) X Fan, M Medved, JN River, M Zamora, C Corot, P Robert, P Bourrinet, M Lipton, RM Culp, and **GS Karczmar**. New model for analysis of dynamic contrast-enhanced MRI data distinguishes metastatic from nonmetastatic transplanted rodent prostate tumors. Magnetic Resonance in Medicine **51**:487-94, 2004.

4) S Foxley, M Medved, M Zamora, C Yang, **G Karczmar**. Fourier component images of rodent prostate cancers show unique morphology pre- and post-contrast , Manuscript in Preparation

Conference presentations: Our work is increasingly useful to the scientific and medical communities as evidenced by frequent invitations to me and my collaborators to give presentations. The following are recent presentations at international conferences:

1) Medved M, River JN, Zamora MA, Corot C, Robert P, Bourinet P, Lipton MJ, Karczmar GS. Differentiation of Metastatic and Non-metastatic Rodent Prostate Cancer Using a New Mathematical Model to Fit Dynamic Contrast Enhanced MRI Data, Twelfth Scientific Meeting and Exhibition of ISMRM, Kyoto, Japan, May 2004

2) Foxley S, Zamora M, River J, Fan X, Karczmar GS. The use of high spatial and spectral resolution Fourier component difference images to detect BOLD response in mouse tumors. Accepted for presentation at the ISMRM meeting in Miami, 2005.

3)Karczmar. New functional and anatomic MR imaging approaches to detection and staging cancer; implications for targeted therapy. Japan/US Cancer Therapy Symposium (JUCTS) on "New Horizons of Targeted Treatment in Radiation Oncology", Maui, Hawaii, 2005

4)Karczmar. Vascular properties of tumors measured using intrinsic MRI contrast. ISMRM Cancer Imaging Course, Miami, Florida, 2005.

– Degrees obtained that were/are supported by this award;

Weiliang Du, PhD. In Medical Physics 2003

Sean Foxley, Ph.D. in Medical Physics expected in 2007.

– Funding awarded based in part or completely on work supported by this award; Over the past two years significant new funding has been awarded based in large part on the pilot studies completed with support from the Army.

Grant #1 R01 EB003108-01 from NIH (P.I. Karczmar); Funding period 09/15/03-07/31/07
High Spectral/Spatial Resolution Imaging Breast Cancer

Grant # 2 R01 CA078803-04A2 from NIH (P.I. Karczmar); Funding period 09/01/99 - 2/29/08
Fast Spectroscopic MR Imaging of Breast Cancer

Grant # R21CA100996 from NIH (R21/R33 – P.I. Karczmar); Funding period 04/15/05 – 04/13/09
Measurement of Subvoxel Microvessel Density With High Spectral and Spatial Resolution MRI.

NIH R21; *Dynamic spatial and spectral, contrast enhanced MRI of breast. This application received as core of 151 and we were informed that funding is highly likely. Although the work will relate primarily to breast cancer it is a direct outgrowth of our work on prostate cancer, and will impact future work on prostate cancer*

CONCLUSIONS: Our results to date demonstrate quantitatively that there are significant advantages associated with high spectral and spatial resolution imaging of the prostate. We have demonstrated that HiSS images of rodent and human prostate show anatomic features that are not visible in conventional images. A new approach to MR imaging – that we refer to as Fourier Component Imaging – has potential to improve delineation of tumor vasculature.

REFERENCES:

1. Kovar, D. A.; Al-Hallaq, H. A.; Zamora, M. A.; River, J. N.; Karczmar, G. S. Fast spectroscopic imaging of water and fat resonances to improve the quality of MR images. Acad Radiol 5(4):269-275; 1998.

2. Kuperman, V.; River, J. N.; Karczmar, G. S. High Resolution Spectroscopic Images of Tumors. International Society for Magnetic Resonance in Medicine ; 1995.

3. Al-Hallaq, H. A.; Zamora, M.; Fish, B. L.; Farrell, A.; Moulder, J. E.; Karczmar, G. S. MRI measurements correctly predict the relative effect of tumor oxygenating agents on hypoxic fraction in rodent BA1112 tumors. Int J Radiat Oncol Biol Phys in press; 2000.

4. Al-Hallaq, H. A.; Karczmar, G. High resolution 1H spectroscopic imaging of the water and fat resonances in human breast. International Society for Magnetic Resonance in Medicine 2; 1997.

5. Al-Hallaq, H. A.; River, J. N.; Zamora, M.; Oikawa, H.; Karczmar, G. S. Correlation of magnetic resonance and oxygen microelectrode measurements of carbogen-induced changes in tumor oxygenation. Int J Radiat Oncol Biol Phys 41(1):151-159; 1998.

6. Karczmar, G. S.; Fanl, X.; Al-Hallaql, H. A.; Zamora, M.; River, J. N.; Rinker-Schaeffer, C.; Zaucha, M.; Tarlo, K.; Kellar, K. Uptake of a Superparamagnetic Contrast Agent Imaged by MR with High Spectral and Spatial Resolution. Magnetic Resonance in Medicine 43:633-639; 2000.

7. Fan, X.; River, J. N.; Zamora, M.; Tarlo, K.; Kellar, K.; Rinker-Schaeffer, C.; Karczmar, G. S. Differentiation of Non-Metastatic and Metastatic Rodent Prostate Tumors with High Spectral and Spatial Resolution MRI. Magnetic Resonance in Medicine in press; 2001.

8. Karczmar, G.; X Fanl, H. A.-H.; River, J.; Tarlo, K.; Kellar, K.; Zamora, M.; Rinker-Schaeffer, C.; Lipton, M. J. Functional and Anatomic Imaging of Tumor Vasculature: High Resolution MR Spectroscopic Imaging Combined with a Superparamagnetic Contrast Agent. Academic Radiology in press; 2001.

9. Oikawa, H.; Al-Hallaq, H. A.; Lewis, M. Z.; River, J. N.; Kovar, D. A.; Karczmar, G. S. Spectroscopic imaging of the water resonance with short repetition time to study tumor response to hyperoxia. Magn Reson Med 38(1):27-32; 1997.

10. Sarkar, S.; Heberlein, K.; Metzger, G. J.; Zhang, X.; Hu, X. Applications of high-resolution echoplanar spectroscopic imaging for structural imaging. J Magn Reson Imaging 10(1):1-7; 1999.

11. Zhong, J.; Kennan, R.; Schaub, M.; Gore, J. C. Measurements of transient contrast enhancement by localized water NMR spectroscopy. J Magn Reson B 104(2):111-118; 1994.

12. Zhong, K.; Li, X.; Shachar-Hill, Y.; Picart, F.; Wishnia, A.; Springer, C. S. Magnetic susceptibility shift selected imaging (MESSI) and localized (1)H(2)O spectroscopy in living plant tissues. NMR Biomed 13(7):392-397; 2000.

13. Posse, S.; Wiese, S.; Gembris, D.; Mathiak, K.; Kessler, C.; Grosse-Ruyken, M. L.; Elghahwagi, B.; Richards, T.; Dager, S. R.; Kiselev, V. G. Enhancement of BOLD-contrast sensitivity by single-shot multi-echo functional MR imaging [In Process Citation]. Magn Reson Med 42(1):87-97; 1999.

14. Posse, S.; Dager, S. Using Functional Proton Spectroscopic Imaging. International Society for Magnetic Resonance in Medicine ; 1995.

I. Abstract

Copenhagen rats bearing metastatic rat prostate AT6.1 tumors inoculated in the hind leg were images using an echo-planar spectroscopic imaging sequence. Imaging was performed with high spectral and spatial resolution in a small bore 4.7T magnet. K-space data from each small voxel imaged were Fourier transformed along the time axis to produce spectra containing a water peak. Typical work thus far in this lab has focuses on the water peak as the source of image contrast and has relied on information obtained from subsequently produced water peak-height images. However, because we are able to obtain both high spatial and spectral resolutions we can analyze the details of the water line width; this allows us to observe non-lorentzian broadening of the peak. By producing 3D data sets in which the water peak for each 2D spatial position is positioned in the same 1D spectral bin we are able to produce images which are comprised solely of the off resonance spectral data points (Fourier component images). If for some specific physiological or anatomical reason there is an inhomogeneous broadening of an ROI of voxels' respective water lines, we will see an associated contrast in these Fourier component images (FCI's) that is not visible in the peak height image. Often such broadenings occur as a shoulder on either side of the peak; however, in many instances there is a splitting of the water peak, producing an off-resonance peak. By producing such FCI's we were able to isolate features in the tumor that were not visible in the on resonance FCI – which is the peak height image. Further, by determining the deviation of symmetry for each bin off resonance from a lorentzian water line we were able to demonstrate that spectra from the tumor displayed greater asymmetry than those of the normal tissue and that the regions in the tumor that showed the greatest differences

changed with the addition of contrast agent. These differences between the baseline and post-contrast asymmetry images revealed different information than the PH difference images.

II. Introduction

Recent and on going work from this lab (*site refs*) utilizes an EPSI pulse sequence to perform a much more efficient method of spectroscopic imaging as compared with more conventional methods while maintaining comparable image metrics (*Weiliang paper*). Spectroscopic data is collected for each tiny voxel in the image slice with high spatial and spectral resolution (HiSS imaging). While this is not, in and of itself, a new concept (*Mansfield ref*), it is only with the recent manufacturing of gradients capable of performing such rapid switching of large gradients strengths that the use of such a pulse sequence has become reasonably plausible and efficiently applicable.

After EPSI data is collected and reconstructed in to a 3d k_x x k_y x t dataset, the matrix is Fourier transformed in both spectral spatial dimensions and along the time axis to produce a spectrum for each spatial data point, corresponding to a small voxel. It is common practice to find the water peak for each voxel and assign that value to its spatial location, thus producing a water peak height image (*find a PH production reference*). However, there is likely more information in the spectrum that is useful and different than that which is contained in the peak height alone. Such information could lay in the off resonance components of the spectrum, indicated by the broadening of the water line. A pure absorption spectrum of a voxel containing only water would produce a Lorentzian water line (*find ref*). Such a distribution is symmetric about the peak. If there are sub-voxelar dimensioned components in the voxel which have different magnetic susceptibilities than water, they would introduce a slight variation in the local magnetic environment (*find ref*). Such variations could produce slight frequency offsets of the local spins; if this occurs in sufficient quantity, this could result in a measurable signal at

a frequency that is slightly off that of the water resonance. This would subsequently produce an inhomogeneous broadening of the water line about the peak in the form of a shoulder or another peak to either side of the water peak.

It has been reported that such inhomogeneous broadening of the water line can be utilized as a new source of image contrast (*Milica ref*). By examining the various Fourier component images of the spectral data, we find that there are visible features that are associated with inhomogeneously broadened line widths that are not visible in the peak height image. These features appear to occur in a very small window of frequencies from case to case, often times at the same spectral distance (in Hz) off resonance, suggesting that they are indicative of some specific feature, either physiological or anatomical. Further, we find that such effects are most dramatic in the tumor as opposed to the normal tissue of the rat's leg. This would suggest that the tumor microenvironment is much more heterogeneous (*find ref*) than the normal tissue. It is the purpose of this work to explore these off resonance components and determine the statistical validity of their existence.

III. Methods

Animal Preparation

All procedures were performed according to protocols approved by the Institutional Animal Care and Use Committee and were in compliance with the Animal Welfare Act and NIH Guide for the Care and Use of Laboratory Animals. AT6.1 metastatic rat prostate tumor cells were inoculated subcutaneously in to the hind limbs of Copenhagen rats (n=5). Tumors were imaged approximately three weeks after inoculation with volumes ranging from 0.5 to 3.0cm^3.

During the MR experiments, mice were anesthetized with 2% Isoflurane gas mixed with medical air (2 liters/minute) and oxygen (0.2 liters/minute) delivered through a mask. Each rat's temperature was maintained by blowing warm air into the bore of the magnet and monitored with a rectal temperature probe. Both heart and respiration rates were monitored as well (Fisher Scientific, Springfield, NJ). A catheter was inserted in to either the jugular or the tail vein for the delivery of the contrast agent. 0.4cc of the agent was delivered for each experiment.

The contrast agent used (Vanadyl acetylacetonate – $VO(acac)_2$) was an experimental agent that is a derivative of the commonly administered Gd-DTPA. This is believed to be a blood pooling agent, so the rate of uptake in to the extravascular, extracellular space is extremely slow. Research is currently being conducted to fully determine its properties and is beyond the scope of this text.

Data Acquisition

Imaging was performed with a 33cm horizontal bore, 4.7 Tesla MR scanner (Omega; GE/Bruker, Fremont, CA) with 20cm bore self shielded gradient coils (max

gradient strength: 100mT/m). A specially designed small four turn Helmholtz coil was used for excitation and detection. All EPSI scans were performed with a 64 lobe readout gradient echo train sampled for 126ms, yielding a spectral resolution of ~7.9Hz. Phase encoding and each lobe of the readout echo train were sampled 256 times over a 4cm field of view, yielding a ~156μm^2 spatial resolution. In all cases, three 1mm slices through the leg were taken to provide a large variation in tumor morphology from a single experiment.

Typically 4-6 baseline scans were performed followed by contrast injection. Post contrast images used for this study were taken immediately after injection injection.

Fourier Component Images

All data processing and subsequent analyses were performed using IDL (RSI, Boulder, CO). Acquired K-space data was encoded in to 3D matrices (k_x x k_y x k_t) and Fourier transformed in each direction to produce a spectral data set for each spatial position. Modulus spectra were produced from the real and imaginary components of these spectra. Each ~508Hz bandwidth spectra were sampled in to 64 data points. The location of the water peak for each voxel was determined and shifted to the center of the spectral window (bin 31 in the 3D dataset). With this shift, the 31st bin of the 3D spatial/spectral dataset was now specifically designated as the position of water resonance and could be viewed as the water peak height image. Each subsequent frequency bin above or below the 31st (multiples of ±7.9Hz) was then also necessarily aligned in such a way that each spatial point had the same frequency offset from resonance as every other one for every spectral bin (figure 1). In this way, we could easily view each off resonance FCI by simply looking at each of the 256x256 point

spatial matrices for each of the 64 spectral components in the dataset. Note that by this method we find that the PH image is just a specific case of a more generalized method of producing Fourier component images.

Asymmetry Images

After producing the 3D FCI datasets, we were interested in determining how inhomogeneous the line width broadening was. If a spectrum was a pure lorentzian then the value of symmetric points about the peak would have the same value (within the noise level). If one were to plot symmetric points about the lorentzian peak against each other the result would be a straight line along x=y. If the spectral water line were inhomogeneously broadened, however, the result would be much different; the points corresponding with the asymmetric broadening of the lorenztian would lie off the line x=y by some distance. The perpendicular distance that the point would lie that line would be a direct measure of the extent of inhomogeneous broadening of the water line; the greater the distance, the more sever the deviation from symmetry. By creating such a symmetry plot for each bin of every voxel in the 3D EPSI data set we were able to produce asymmetry images (AIs) for each off-resonance point of the spectrum. Because the water line is vary narrow, only AIs for the first three points off resonance were produced.

PH vs. Asymmetry difference mask images

In order to compare the regions of greatest change between the PH difference images and the asymmetry difference images, thresholded masks of each were produced. A mask of each slices' PH image was created by thresholding by 2 standard deviations (to remain consistent with the asymmetry thresholding) of the distribution of difference

values. Because we are only interested in the regions of greatest change but not the actual amount, negative differences were simply assigned a value of -1, and positive values, 1. In order to specify that only clustered pixels remain, and not noise, which could confound the statistics of the overlap between the PH difference and the asymmetry difference, a 2x2 pixel filter was passed used to delete any pixels that were in clusters of 2x2 or smaller. The same procedures were followed for each asymmetry difference image for each bin off resonance for the same slice. Pixels that correspond to a change that was above the threshold in both the PH difference image and the asymmetry difference image were determined and counted.

IV. Results

Fourier component images

Indicative FCI images are shown in figure 2. In order to ensure that all images were windowed the same, each point of each FCI, including the PH image, were normalized by its respective mean value. This ensured that the data points near the mean value of each image were approximately the same, for all FCI's. In doing this we were able to make intra-FCI comparisons based on different pixel values alone, ensuring that purely qualitative comparisons were based on real changes in contrast and not just an issue of scaling. We found that the most usable off resonance spectral components occurred up to and including ±~31.6Hz away (4 bins off resonance) from the location of the peak height. Features are clearly visible in these FCIs that are not present on resonance. Some structures of note are the thin squiggly lines that appear throughout the tumor. We believe that these could be vasculature.

Asymmetry plots

The general spectral feature that we are most interested in when producing FCIs is the characteristic broadening of the water line width associated with specific features in a tumor. By examining the symmetry of the spectrum, we can effectively produce yet another type of image that is a direct consequence of the FCIs. By plotting symmetric bins of the water peak against one another, we can estimate how much each component of the spectrum deviates from the symmetric lorentzian. This is done by recognizing that if the spectra of all of the voxels in the slice from which the data was collected were pure lorentzians that the resultant symmetry plots would be straight lines along $x = y$ (±some standard deviation due to noise). However, if one side of the spectrum was

inhomogeneously broadened, the resultant point on the plot would fall some distance above or below the line. By plotting all points of each symmetric set of off resonance components and calculating the distance of the point from the line we are able to estimate the degree of asymmetry associated with each bin off resonance. Such typical distance images are displayed in figure 3. We find that the greatest source of asymmetry that it is localized predominantly to the tumor is in the first three bins off resonance. Of the 5 experiments, with three slices each, we can consider 15 baseline and 15 post contrast images per off-resonance bin (for a total of 30 scans per bin). The greatest asymmetry (both in that it occurred with the greatest distance from the line x=y and that it was highly clustered) occurred in the tumor in 28, 25, and 22 of the 30 images, for bins 1, 2, and 3, respectively.

Asymmetry subtraction images

Because each FCI image was normalized by the mean of itself, we are able to compare different scans of the same symmetric spectral components. This allows us to perform a direct comparison between the pre and post contrast injection AIs. By subtracting the average baseline AI from the corresponding post contrast AIs, we find that there is a systematic effect on the symmetry of the spectra due to the introduction of the contrast agent. Of the five experiment, in which three slices were imaged in each, and including the first three bins off resonance (for a total of 45 AI difference images), 40 cases showed that the greatest relative difference (both positive and negative) occurred in the tumor. More specifically, we found that 14 of the 15 first bin off-resonance, 14 of 15 of the second bin off-resonance, and 12 of 15 of the third bin off resonance showed this effect. In 40% of these cases we found that leg showed large differences as well,

however, these differences in the leg appeared mottled, whereas the differences in the tumor were clustered. Further, the instances of large mottled differences in the leg increased as we looked further off resonance (4 cases displayed excessive leg mottle in the first bin whereas 9 cases displayed it in the third bin). This is likely because the water line in very narrow, so as we look further off resonance, noise becomes more and more of a factor. As we looked further off resonance than the third bin, the greatest differences in all cases appeared evenly distributed across the leg and the tumor. While technical challenges exist in verifying the correspondence of exact spectral components with anatomy and/or physiology, we are able to make the observation that the spectrum is most affected by the contrast agent in the tumor and at frequencies just off resonance.

Comparing the baseline asymmetry images with the post-contrast we found that, in general, the regions of greatest asymmetry were approximately the same. The overlaps between the baseline and post-contrast were 43.2±13.5%, 46.2±13.1%, and 47.1±10.0% for bins 1, 2 and 3, respectively. Note that the difference in overlap is due to increases and decreases of clusters of asymmetry in the same regions of the tumor. This is in stark contrast with the overlap between the differences between these and the PH difference images.

PH difference image vs. ADI difference images

The information obtained in the PH difference images is specific to how the contrast agent changed the spectral peak height and reflects regions of the tumor in which this was significant. We also showed that off resonance components are affected by the contrast agents as seen in the asymmetry difference images (ADIs). Interestingly, the regions in the tumor that showed the greatest differences in ADIs do not correlate with

the regions of greatest difference in the ADIs. This can be seen in figure 4. Difference images of both types were thresholded by two standard deviations of their own distributions of values so that only the greatest absolute difference pixel values remained. Masks of each were produced where negative differences were assigned a value of -1, and positive differences a value of +1. Pixels that corresponded between PH difference images and ADIs were subsequently determined and shown in blue. Note that the correspondence was for absolute pixel values, so consideration for positive or negative differences were not made. We see in the figure that there was little overlap of the three bins of ADIs compared with the PH image. Over all five experiments and each of the three slices in each we found that the maximum amount of overlap (20.5±6.9%) between PH difference images and ADIs occurred in the first bin off-resonance for the baseline scans; the minimum occurred in the third bin post-contrast with an overlap of 16.7±5.2% of pixels, which could be due to a coincident increase in mottle in the post contrast ADI.

V. Discussion

By examining the off resonance features of the spatial/spectral data obtained using HiSS, we are able to detect features in the tumor that are not present in the PH images. While future work is required to determine what these features could be, either physiological, or anatomical, it is likely that they are the direct result of changing magnetic environments in the micro structure of the tumor.

FCIs allow us to examine these effects as a direct consequence of a change in signal at each off-resonance component. Such changes are likely confined to specific anatomical or physiological features of the tumor. One such example would be tumor vasculature. If features of the tumor could be correlated with the off resonance components with some degree of certainty, we could start to perfume more accurate observations of these features than would be available to the PH image or more conventional imaging techniques.

By examining the asymmetry of the spectra we are able to find out even more about the off resonance information than by just looking at the FCIs. We know that the spectral line is proportional to the inverse of T_2^*. If it decreases we would see a homogeneous broadening of the line width. By looking solely at the FCIs, we would not necessarily be able to distinguish this from an effect due to inhomogeneous broadening. However, if we examine the symmetry of the water line as well, we would be able to discriminate between changes in contrast in FCIs that were due to characteristic broadening associated with T_2^* and those that are due to changes in local magnetic field, producing shoulders or peak splitting. This is because a broadening due to a decrease in T_2^* would not deviate more than the noise from the line x=y when symmetric points were

plotted against one another. So by simply determining the symmetry of the spectra for each voxel in a 3D HiSS data set, we are able to enrich our understanding of the features that are present in FCIs that are not present in the PH images.

We believe that many of the features that are present in the FCIs are due to vasculature. Blood, as demonstrated by the BOLD effect, has some magnitude of magnetic susceptibility that can produce local field inhomogeneities. It would seem reasonable to assume that with high enough spatial and spectral resolution that these field inhomogeneities would be enough to produce detectable slight frequency offsets in the spins at or near vasculature. Because of the dense and erratic vasculature that exists in tumors, it would be plausible that they would be detectible. Interestingly, if we compare the pre and post contrast asymmetry images, we find that the action of the contrast agent on these is to change the degree of asymmetry in the same regions of the tumor as were found to be asymmetric in the baseline images. We believe that the contrast agent is a blood pooling agent, which means that it tends to remain in the vasculature for a long time. These two points combined would suggest that the features detected in the tumor that are indeed related to the concentration of vasculature in the voxel. Further work will need to be performed to explore this possibility, however.

By looking at these various components of the spectra we find that there is a very rich supply of information that we cannot obtain by looking at the peak height image alone, and that is not available to more conventional imaging techniques.

FIGURE 1

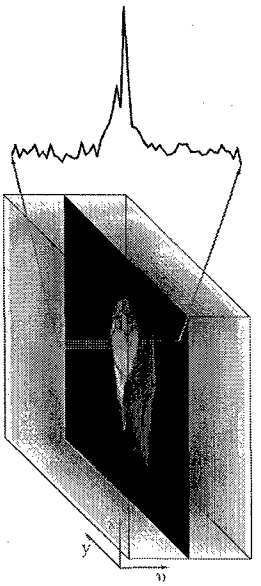

FCI images are created in such a way that the peak of each spectrum for each tiny voxel is aligned in the same bin. This ensures that the same off resonance peaks are aligned in the same bin as well, and off resonance Fourier component images can be produced.

FIGURE 2

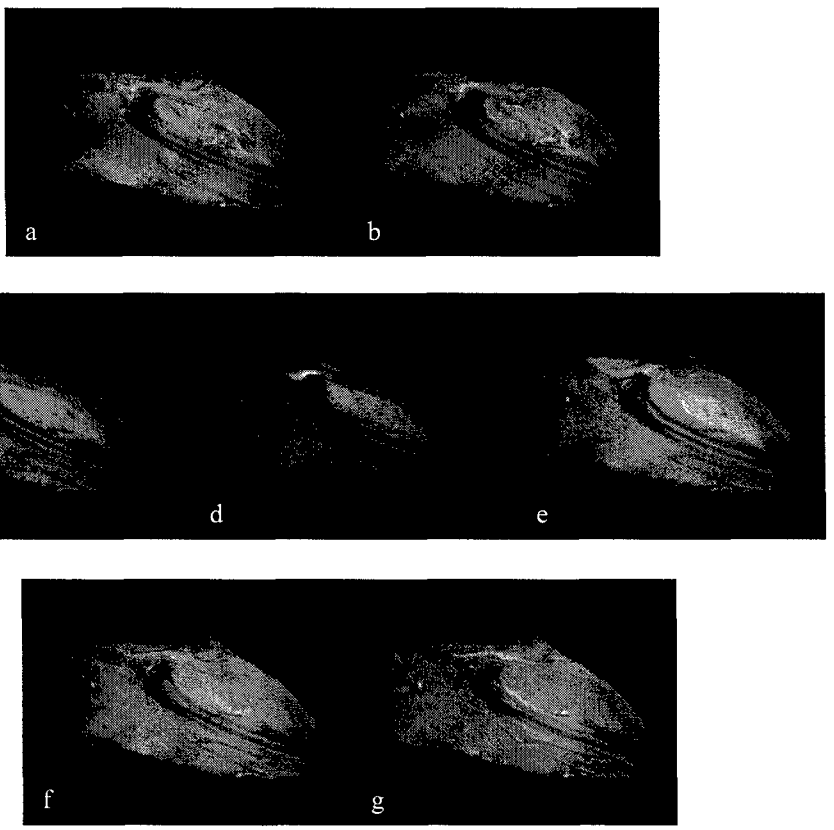

Images are FCIs three bins to the left and three bins to the right of the PH image (the central bin FCI - d). The tumor is clearly visible in the PH image. Notice the changes in tumor morphology from FCI to FCI. Increases in signal in off-resonance FCIs are likely due to inhomogeneous broadening of the water line. Some contrast could be due to changes in T_2^*, however, this would appear in multiple FCIs and in both directions from the PH image. More abrupt contrast changes between FCIs could be due to either spectral shoulders or secondary peaks.

FIGURE 3

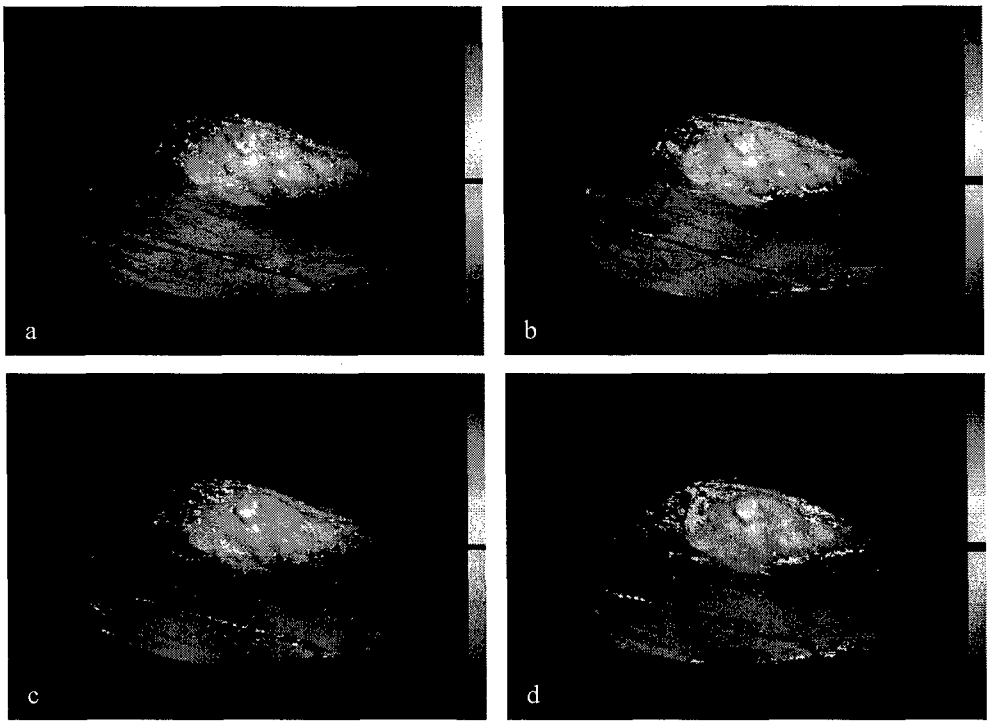

(a-b) Baseline Asymmetry distance images for the first and second bins off-resonance, respectively.
(c-d) Post-contrast Asymmetry distance images for the first and second bins off-resonance, respectively.
All images were thresholded by a value equal to two standard deviations of its distance value distribution and are superimposed on the corresponding PH image. Note that the maximum and minimum of each relative scale is symmetric about zero

FIGURE 4

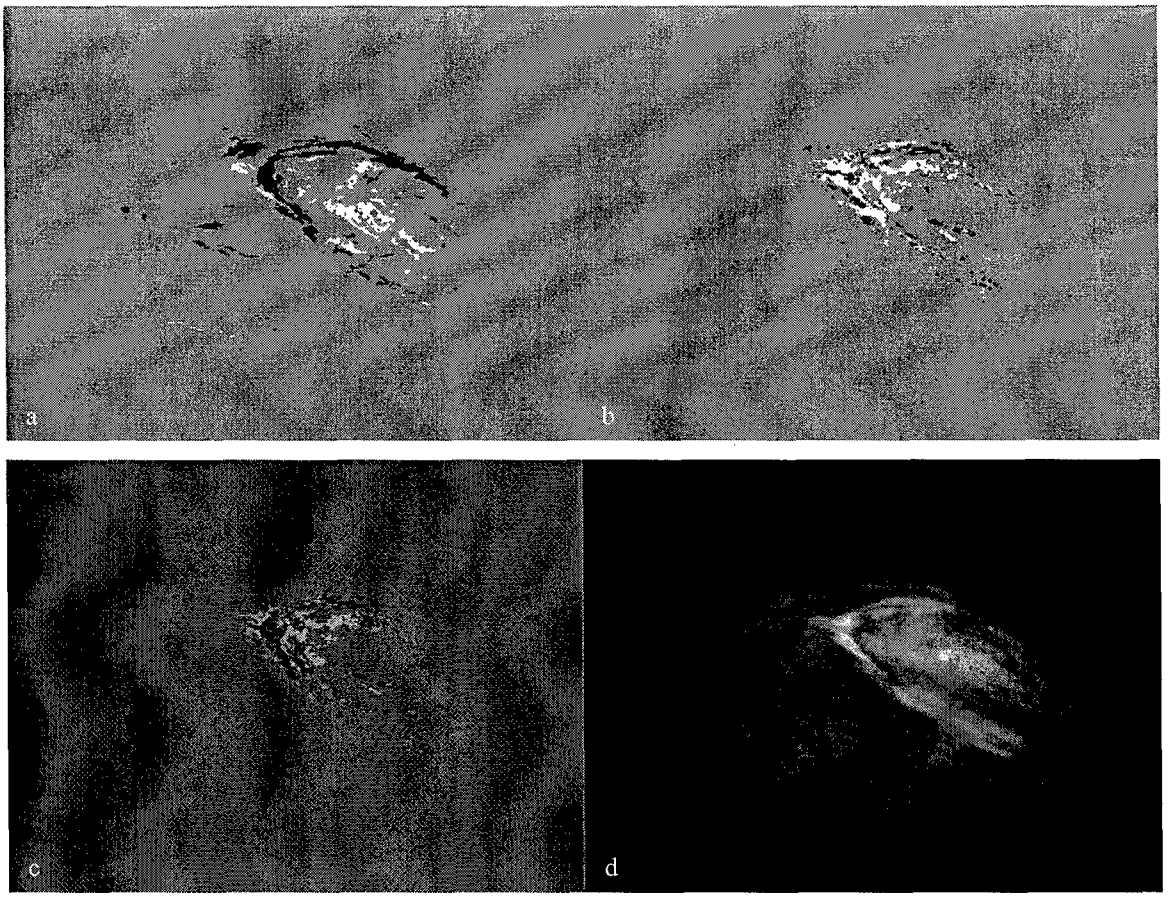

(a) Thresholded PH difference image (2 standard deviations of the distribution of the PH difference values). Black indicates a negative change; white, a positive change. Actual values were masked out to clearly illustrate the point of overlap between the PH difference image and the AI difference image.

(b) Thresholded Asymmetry difference image. The image was masked the same as the PH difference image.

(c) The same as (b) but the overlap of the PH difference image is superimposed in blue. The overlap is independent of the sign of the difference, but rather indicates locations of simultaneity.

(d) The corresponding PH image.